Ecology Letters

WILEY

ECOLOGY LETTERS

LETTER

Density Dependence Shapes Life-History Trade-Offs in a Food-Limited Population

Harman Jaggi[1] | Wenyun Zuo[1] | Rosemarie Kentie[2,3] | Jean-Michel Gaillard[4] | Tim Coulson[5] | Shripad Tuljapurkar[1]

[1]Department of Biology, Stanford University, Stanford, California, USA | [2]NIOZ Netherlands Institute for sea Research, Den Burg (Texel), The Netherlands | [3]Institute for Biodiversity and Ecosystem Dynamics, University of Amsterdam, Amsterdam, The Netherlands | [4]Laboratoire de Biométrie et Biologie Evolutive, Université Lyon 1, CNRS, UMR 5558, Villeurbanne, France | [5]Department of Biology, University of Oxford, Oxford, UK

Correspondence: Harman Jaggi (harmanjaggi@stanford.edu)

Received: 20 March 2024 | **Revised:** 12 September 2024 | **Accepted:** 13 September 2024

Editor: Juan Manuel Morales

Funding: The authors received no specific funding for this work.

Keywords: density dependence | density-dependent selection | life history | LRS | trade-offs | trait covariation

ABSTRACT

Quantifying trade-offs within populations is important in life-history theory. However, most studies focusing on life-history trade-offs focus on two traits and assume trade-offs to be static. Our work provides a framework for understanding covariation among multiple traits and how population density influences the traits. Using detailed individual-based data for Soay sheep, we find density strongly shapes life-history trade-offs and distribution of lifetime reproductive success (LRS). At low density, a trade-off between juvenile survival and growth structures life-history variation, whereas at equilibrium density, trade-off between reproduction and juvenile survival is the major structuring axes. Contrary to Lomnicki's prediction, we find that at high density, there is little variation in the LRS over the sizes (large juveniles and adults) that contribute to reproduction. Our results advance an understanding of dynamic nature of trade-offs offer insights into how high-density limits diversity of individual life histories and have implications for evolution via density-dependent selection.

1 | Introduction

There is tremendous variation in life-history strategies (Roff 1992; Stearns 1992). The evolution of these strategies is known to be constrained by physiological limitations and in food-limited populations by trade-offs in resource allocation (Stearns 1989; Descamps et al. 2016). Evolutionary theory posits that organisms must allocate limited resources towards different suites of traits to optimise their fitness. Despite evidence for trade-offs, for example, offspring size/number (Smith and Fretwell 1974; Venable 1992), immunocompetence and life-history traits in birds (Norris and Evans 2000), trade-offs observed in natural systems are less ubiquitous than those hypothesised by life-history theory (Metcalf and Jessica 2016). Trade-offs may be difficult to detect because individual variation in resource acquisition is often larger than variation in resource allocation (Van Noordwijk and De Jong 1986), thereby masking life-history constraints in empirical studies. Although life-history theory predicts costs of reproduction and therefore negative correlations among certain traits, individuals can show positive, negative or zero correlations (due to stochasticity) while simultaneously being involved in a classical physiological trade-off (Bell and Koufopanou 1991; Horvitz, Schemske, and Caswell 1997; Zera and Harshman 2001; Hodgson and Townley 2004; Descamps et al. 2016).

Whether trade-offs within a population are static or change with environmental or demographic conditions is an

important question. For instance, as population density varies, individual fitness (ability to survive and reproduce) may also vary further impacting life-history outcomes. This could result from chance encounters with potential mates or competitive individuals. Further, life-history and physiological mechanisms operating at low density may differ from those operating at high density (under intense resource limitation), altering the nature and direction of trade-offs. Thus, variation in population density can generate time-varying selection for different life-history strategies, via density-dependent selection. The concept that selection of life-history traits could vary with population density has been discussed both empirically and in theory by Dobzhansky (1950), MacArthur (1962), and Roughgarden (1971). Pianka (1970) proposed the $r-K$ selection continuum, where r (that refers to intrinsic population growth rate) corresponds to strategies that maximise productivity (i.e., putting all energy into reproduction and producing more offspring) at low density and K (that refers to equilibrium carrying capacity) corresponds to strategies that maximise efficiency (i.e., putting most energy into survival prospects, competitive ability and producing few offspring).

This brings us to our central question: how do we understand life-history variation at different densities while identifying life-history trade-offs? Although we tend to think of trade-offs and density dependence separately, we show here that they are intimately linked. We examine trade-offs by performing a Principal Component Analysis (PCA) on specific vital rates (such as survival, reproduction and proportional growth increment), defined in the methods section. Previous studies (Czesak and Fox 2003; Agrawal, Conner, and Rasmann 2010) have primarily focused on covariation between two traits but in our research, we examine trade-offs among multiple traits by considering the exceptionally detailed long-term observational data collected on Soay sheep (*Ovis aries*) in the St. Kilda archipelago, Scotland. The sheep system is of special interest because this population has been shown to fluctuate dramatically thereby exhibiting potential for density-dependent selection. Coulson et al. (2001) noted population declines of up to 60% occurred when population size was large and winter weather was harsh. This is due to non-linear interactions between winter weather, population's response to changes in density and food availability (Grenfell et al. 1992; Clutton-Brock et al. 1996; Coulson et al. 1999).

Our first result shows that density dependence shapes life-history trade-offs in a food-limited population of a large herbivore. At low densities, we find negative correlations between survival and growth during the juvenile stage. However, the intensity and strength of the negative association between juvenile survival and growth increases with increasing population density. Interestingly, at equilibrium capacity (K), new trade-offs appear and strong negative association between reproduction and juvenile survival structures life-history variation within the population. We find that changes in population density affect the relationships among vital rates such as survival, growth and fecundity. The strength of density-dependent responses of vital rates varies a lot, resulting in trade-offs. Our findings are consistent with life-history theory (Stearns 1992), which predicts trade-offs prevent individuals from being proficient at both surviving and growing to large sizes. Kentie et al. (2020) found Soay sheep individuals with an optimal life history strategy at high density were different to those having an optimal strategy at low density. Individuals could not maximise fitness in both high- and low-density environments.

Next, we examined the effects of density on variation in demographic measures. The demographic measures of interest are variation in average vital rate functions, net reproductive rate R_0, and stable age-stage distribution (SSD). We also calculated the distribution of lifetime reproductive success (LRS) using Tuljapurkar et al. (2020) to tease apart trade-offs between allocation in survival and future reproduction. LRS is an important component of individual fitness and previous studies have revealed that LRS distributions are often non-normal and highly skewed (Cabana and Kramer 1991; Tatarenkov et al. 2008). This begs the question: does the distribution of LRS and the skew remain consistent across all population density regimes?

Our research predicts density dependence strongly affects the distribution of LRS. We also find the distribution of LRS is highly constrained at high densities as noted by the empirical confidence intervals at different densities. In particular, it is the females at prime adult size (~21 kg) that contribute the most at high densities, whereas at low densities contributions come from a wider range of body size (~12–21 kg). Lomnicki's (1978) work hypothesised a higher variation in vital rates and demographic outcomes (such as LRS) among females at high density compared to low density. They predicted increasing complexity in life history variation at the highest density. However, our results suggest the opposite to be true for Soay sheep as we find individual differences are more pronounced at low density compared to high density. We find a similar pattern for average vital rate functions and stable stage distribution. We base our model and results on previously published Integral Projection Model (IPM) and delifing method presented in Coulson et al. (2006), Coulson (2012) and Kentie et al. (2020).

Characterising trade-offs as a function of population density can not only help elucidate the various determinants of observed life-history variation but will also determine what strategies may be most important for population persistence. Our framework is general and can be adopted for species with individual life-history data, such as *Hypericum cumulicola* (Quintana-Ascencio and Morales-Hernández 1997), *Heliconia acuminata* (Brooks et al. 2019) and *Poecilia reticulata* (Reznick, Bryant, and Holmes 2006; Bassar et al. 2016). We tabulate (Table 1) a summary of our approach to perform the analysis for other species with individual life-history data. The work allows us to examine trade-offs, and variation in LRS at low and high densities and comment on how density dependence can operate.

2 | Model and Methods

We begin with defining the Integral Projection Model (IPM) for Soay sheep and then describe sampling of life histories to evaluate trade-offs and the distribution of LRS. IPMs are structured population models that use linear (or linearised) regressions to describe the expected phenotypic trait trajectories (Coulson 2012; Ellner, Childs, and Rees 2016). The IPM consists of four functions that describe how traits such as body size (z) influence survival, reproduction, growth and offspring size.

TABLE 1 | Overall framework for identifying trade-offs at different densities.

Step	Description
1. Define and parameterise IPM functions	Identify IPM functions necessary for the study system and parameterise these functions based on the data observations. This step involves specifying the growth, survival and reproduction functions that will be used in the IPM
2. Delifing or leave one out	Implement the delifing method or the leave-one-out technique. This involves iteratively removing one data point and reparameterising the IPM to evaluate the impact of each individual on the model's predictions
3. Covariance matrix and sample life histories	Generate the covariance matrix from the delifing life history data. This matrix captures the relationships between different parameters in the IPM functions. Sample artificial life histories from the multivariate normal distribution defined by the mean vector and covariance matrix obtained from the empirical data
4. Find the carrying capacity (K) for each sample life history	Determine the carrying capacity at which the population growth rate, $r = 0$. This involves running the IPM at different population densities and identifying the density at which the population is at equilibrium
5. Re-evaluate IPM at different densities (e.g., $N = 0, N = K/2, N = K$)	Evaluate the IPM at different population densities. This involves running the IPM functions at varying density levels
6. Principal component analysis to identify trade-offs	Perform a principal component analysis (PCA) on the life history traits of interest (i.e., juvenile survival, adult survival, reproduction and growth) to identify the main axes of variation and potential trade-offs. Our method allows an understanding of covariation among traits within the population at different densities

For Soay sheep survival, transitions and reproduction during a single time interval depend on age and stage (Coulson 2012). We model Soay sheep demography in discrete time with population projection matrices (PPMs) structured effectively by body size (that describes stage) based on (Coulson 2012; Kentie et al. 2020). We say effectively because we add a maximum age of death. That is, we assume that at each age, the size-based matrices have the same survival and fertility rates until the sheep eventually die at a maximum age of death and at this age, the elements of the survival matrix are made all 0. This enables us to construct a block matrix with size-structured matrices for each age. Based on empirical observations, the maximum age of death is set to 16. The individuals are classified into 50 equal-sized stage classes from 1 kg to 38 kg (based on their body size). Since there are 16 ages, the dimension of the block matrix is 800×800 (50 body sizes times 16 age classes).

Note that the models are parameterised using female sheep data since the growth rate of Soay sheep population is known to be female-dominant (Coulson et al. 2001) and there is no limiting effect of the number of males for female reproductive output. We use previously published data and IPM for Soay sheep (Coulson 2012; Kentie et al. 2020). The generalised linear functions for survival and reproduction are as follows and we plot $S(z,t)$ and $R(z,t)$ for different values of N (Figure A2):

$$S(z,t) = \frac{1}{1+e^{-(s_0+s_1 z+s_2 N_t)}}$$
$$R(z,t) = \frac{1}{1+e^{-(r_0+r_1 z+r_2 N_t)}}.$$

Here N_t is the population size at time t. s_0, s_1, s_2 are the intercept, slope and coefficient for body size and density dependence and are our parameters of interest for varying survival. The same holds with r_0, r_1, r_2 and reproduction function. For the parameter values, both survival and reproduction increase with body size z until it eventually saturates.

The growth $G'(z'|z,t)$ and parent-offspring (also called inheritance) $D(z'|z,t)$ functions are described by Gaussian probability density functions. The growth function $G'(z'|z,t)$ is the probability that an individual with body mass z at time t will have a body mass z' at time $t+1$. The parent-offspring function $D(z'|z,t)$ is the probability that an individual with body mass z at time t will produce an offspring with body mass z' at time $t+1$.

$$G'(z'|z,t) = \frac{1}{\sqrt{2\pi\sigma_g^2[z']}} e^{-\frac{(z-E_g[z'])^2}{2\sigma_g^2(z')}}$$
$$D(z'|z,t) = \frac{1}{\sqrt{2\pi\sigma_d^2[z']}} e^{-\frac{(z-E_d[z'])^2}{2\sigma_d^2(z')}}$$

Here $E_g[z']$ is a linear function that predicts expected body mass and similarly $E_d[z']$ predicts offspring's expected body mass at $t+1$ and are given by $E_g[z'] = \gamma_0 + \gamma_1 z + \gamma_2 N_t$ and $E_d[z'] = \delta_0 + \delta_1 z + \delta_2 N_t$. The function describing variance around the expectation $\sigma_g^2(z')$ and $\sigma_d^2(z')$ are also linear and are independent of population density. $\sigma_g^2(z') = \gamma_3 + \gamma_4 z$ and $\sigma_d^2(z') = \delta_3 + \delta_4 z$. The table below summarises the descriptions of our parameters of interest.

We define Growth Increment as average difference in size at time t + 1 and time t divided by the size at time t: Growth Increment, $G = \left(E_g\left[z'\right] - z\right)/z = \left(\gamma_0 + \left(\gamma_1 - 1\right)z + \gamma_2 N_t\right)/z$. The intuition is that individuals reach an asymptotic body size (say y) at which growth increment (G) becomes 0 after 2, 3, or even 4 time steps depending on the age at which individual asymptotic size is reached. We can then partition growth increment until size y (asymptotic body size). The individuals yet to reach their asymptotic size will have a positive growth increment and is denoted by G. We refer to these individuals as juveniles in this manuscript. Note that we partition survival based on individuals who have not yet reached their asymptotic size and denote the average of these individuals as juvenile survival. Soay sheep are determinate growers- they grow from conception to some time on their trajectory when they reach an asymptotic size. From this time onwards, the sheep should not vary much in size on average during the adult stage and we do not consider growth beyond reaching asymptotic size.

We use body mass distributed along 50 size classes as the trait since it is known to affect both survival and reproduction in Soay sheep, and is affected by population density. The IPM functions describe how body size z influences survival, reproduction, growth and offspring size by iterating the distribution of z at t, $n(z,t)$ to $n\left(z', t+1\right)$:

$$n\left(z', t+1\right) = \int \left[D\left(z'|z,t\right)R(z,t) + G'\left(z'|z,t\right)S(z,t)\right]n(z,t)dz$$

where population size is $N(t) = \int n(z,t)dz$. In matrix terms, the IPM can be written as:

$$\mathbf{n}(t+1) = [\mathbf{D}(t)\mathbf{R}(t) + \mathbf{G}(t)\mathbf{S}(t)]\mathbf{n}(t) \quad (1)$$

Using the IPM functions described above, we construct 50 × 50 body size-based matrices for fertility and survival given by $F\left(z', z\right) = D\left(z', z\right)R(z)$ and $P\left(z', z\right) = G'\left(z', z\right)S(z)$ (Steiner, Tuljapurkar, and Coulson 2014). We can construct a matrix $\mathbf{P}_a$ which describes probability that an individual in stage z at age t is alive in stage z' at $t+1$ which is then used to calculate survivorship denoted by $\mathbf{L}_a$. Similarly, we get $\mathbf{F}_a$ matrix which describes the number of stage z' recruits produced by a female of size z at age a. The net reproductive rate R_0 is calculated as the dominant eigenvalue of the matrix $\sum_a \mathbf{F}_a\mathbf{L}_a$. Note that the summation for ages a is until the maximum age of death (set to 16). In addition, we keep the matrices constant for all ages below the age of death which greatly simplifies our analysis. We can do this for different life histories to understand the pattern of variation within the population. Below we describe how we generate many life histories based on Coulson et al. (2006) and Kentie et al. (2020).

2.1 | Average Vital Rates at SSD to Evaluate Trade-Offs

Coulson et al. (2006) introduced an approach called delifing or leave one out to estimate the contribution of an individual to realised changes in population size distribution during a time interval. Using delifing, Kentie et al. (2020) estimated covariance across Soay sheep life-history parameters (such as s_0, s_1, ..., and so on) and examined how fluctuating population densities affect within-population variation in life-history strategies.

In this paper, we first use delifing approach and estimate the covariance matrix (for more description of delifing, refer to Coulson et al. 2006; Kentie et al. 2020). Following this, we sample parameter sets of vital rates spanning possible life-history strategies. A parameter set comprises the 16 parameters: (s_0, s_1, s_2, r_0, r_1, ...) and describes a possible life-history strategy (refer to Table A1). We then substitute parameter values into their respective IPM functions and calculate the population ($N = K$) at which the growth rate (λ) equals 1. The population growth rate λ is the dominant eigenvalue of the age-stage block matrix in Equation (1). Thus, for each life-history (described by a parameter set), we have a corresponding carrying capacity, K. We sample a subset of 250 parameter sets and make further analysis using the sample. Figure A1 shows the range of equilibrium capacity for the 250 parameter sets. The results are robust with respect to the sampling procedure and sample size.

Next, we transform the output of IPM functions (survival, reproduction, growth, and development at each size and age) into covariates for the PCA analysis. To do this, we calculate the IPM functions at each parameter value and at the corresponding density ($N = K$). For survival and reproduction at a given age, we get a vector for the 50 equal sized stage classes from 1 kg to 38 kg. Since the size distribution is different at each density, we weigh survival by the stable size distribution (multiplying with the corresponding SSD at that density). We then partition survival vector into *Juv. Survival* and *Ad. Survival*. *Juv. Survival* is evaluated by averaging annual survival for individuals up to the body size (y) at which growth increment (G) becomes 0 (individual asymptotic size is reached). *Ad. Survival* is consequently the annual survival of individuals of size y. Reproduction is calculated by averaging the annual reproduction of individuals of all sizes. For growth and development, the IPM output is a 50 × 50 size-structured matrix. To transform into a vector, we define the Growth covariate as the average difference in size at time t + 1 and time t divided by the size at time t: Growth Increment, $G = \left(E_g\left[z'\right] - z\right)/z = \left(\gamma_0 + \left(\gamma_1 - 1\right)z + \gamma_2 N_t\right)/z$. We also scale the reproduction and growth vector with the SSD.

This way we generate a dataframe of four average vital rates or demographic covariates of interest (*Juv. Survival*, *Ad. Survival*, *Reproduction*, and *Growth*). Each covariate is an average vector of length 250 (corresponding to the parameter set). Lastly, since K is known, for each parameter set, the IPM functions are evaluated at half the carrying capacity $N = K/2$ and at $N = 0$. We rinse, rather, repeat the above procedure to get dataframes for population size $N = K/2$ and at $N = 0$. The final dataframe for PCA analysis comprises 4 columns and the 750 rows.

To identify trade-offs, we perform a PCA on the average vital rates discussed above at three densities ($N = 0, N = K/2, N = K$). We predict the effects of density by focusing on population $N = 0$, $N = K/2$ and $N = K$. We also explore the results from increasing

the equilibrium capacity beyond $N = K$ as discussed in the Results section.

2.2 | Examining the Variation in LRS

LRS measures the number of offspring an individual produces over its lifespan and individuals may produce 0, 1, 2, ... offspring, until they eventually die. The number of offspring produced during a time interval depends on the age and stage at the beginning of the time interval and is specified by probability distributions of producing 0, 1, 2, ... offspring. The distribution is assumed to be Bernoulli since Soay sheep produce either 0 or 1 offspring in a time interval and we ignore twinning (less than 1.9% of the offspring recruited are twins Simmonds and Coulson 2015). Thus, following Tuljapurkar et al. 2020, we can compute the exact distribution of LRS for the vital rates.

Tuljapurkar et al. (2020, 2021) developed an exact analysis to calculate the probability distribution of LRS for species described by age + stage models. The method assumes the empirical vital rates are known for a large cohort of individuals, for each stage of individuals life cycle. We use the method detailed in Tuljapurkar et al. (2020) to compute LRS distribution of Soay sheep individuals and examine demographic heterogeneities in the distribution.

The mean of LRS distribution is the net reproductive rate R_0. We decompose R_0 into probability of having no offspring and R_0 conditional on making nonzero offspring, denoted by γ and is easily calculated as one minus the probability of reproductive failure (β_0).

$$R_0 = \sum_{k\geq 0} k\beta_k = \sum_{k>0} k\beta_k$$

$$\beta_0 = 1 - \sum_{k>0} \beta_k,$$

where β_k is the probability of having k offspring. We are interested in $\gamma = \sum_{k>0}\beta_k$, which is the mean LRS conditional on reproducing at least once.

3 | Results

3.1 | Trade-Offs and Correlations at Different Densities

Using PCA, we examine the multivariate relationships between life history traits (average vital rates evaluated at SSD). The percentage values in Figure 1 represent the proportion of the total variance explained by each component. Most (between 68% and 80%) of the observed variation in vital rates is explained by the first two principal components. At low density, the variance along the first principal component is explained by the trade-off between survival and growth until individuals reach their asymptotic size. As population density increases, the distribution of the traits is slightly altered compared to $N = 0$, indicating changes in the relationships between traits. As equilibrium capacity ($N = K$), the trade-off between survival and reproduction becomes most significant and structures life-history covariation (Figure A3, sign for reproduction and juvenile survival are opposite). The distribution pattern suggests that the traits are influenced differently by the increased population density.

We validated our results by comparing the individual percentages of variance of the components with the values expected from the broken stick distribution (King and Jackson 1999). The broken-stick model provides a consistent approach to choosing significant principal components as it retains those components that explain more variance than would be expected by randomly dividing the variance. We identified principal components whose associated eigenvalues surpass those predicted by the null model (broken stick) in Figure A5. The variation captured by these components reflects significant underlying patterns in our data and is not a result of chance alone.

We find negative correlation between growth increment and survival for individuals before they reach asymptotic size is present at all densities and corresponds to the main structuring axis of life history variation across individuals (Figures A6 and A4). This association has an increasing importance in shaping life history variation with increasing density and that at high densities, there is a three-way trade-off between survival, growth increment, and reproduction. At high density, juvenile survival negatively correlates with all other vital rates—reproduction, adult survival and growth.

We also examined the demographic consequences when the population density increases beyond the $N = K$ to $N = (1.2)K$ and $N = (1.4)K$ (Figure A7). We find that the trade-off between survival and reproduction weakens as population density is increased beyond K but the growth-survival trade-off remains strong.

3.2 | Variation in Net Reproductive Rate at Different Densities

Having identified the dynamic nature of trade-offs with population density, we examined density effects on demographic outcomes such as the net reproductive rate (R_0) and the stable stage distribution. The R_0 is calculated as the mean of the LRS distribution as well as through the age-stage block matrix (results are consistent).

Figure 2 depicts the decrease in variation in R_0 as a function of population size and we find both mean and variance of R_0 decreases with increasing N. Since both $S(z, t)$ and $R(z, t)$ are monotonically decreasing in N, R_0 is also a monotonically decreasing function of N. The key point here is the extent of variation in R_0 for a density-independent (i.e., at low density limit $N = 0$) and density-dependent case. The life histories with large R_0 at low densities are highly impacted in the sense that such life histories do not exist at high densities and only life histories with low R_0 occur.

What factors contribute to decline in R_0? We examine the distribution of mother's body size at different population densities by calculating the proportion of mothers in each size bracket and the offspring they make. In Figure 3, we find the range

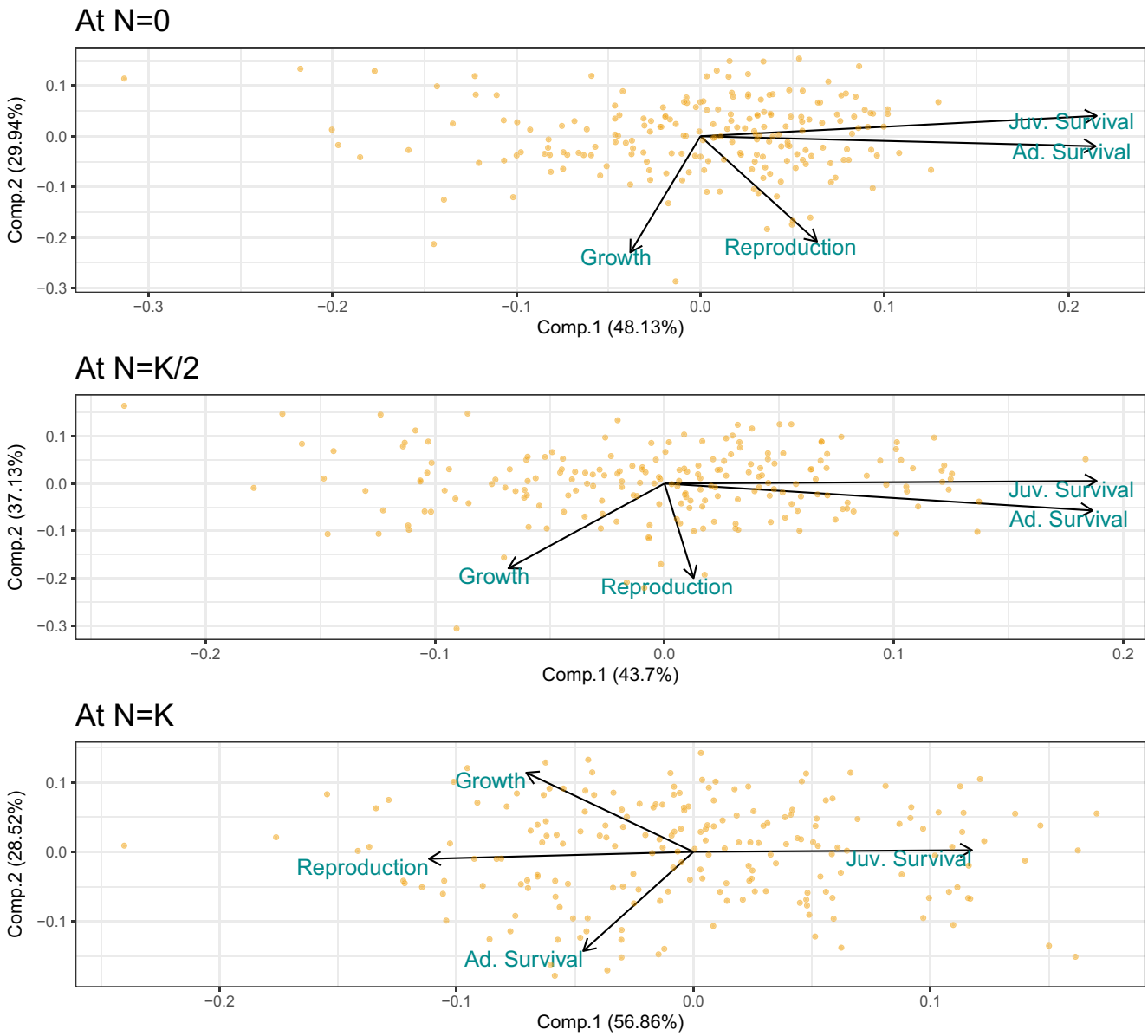

FIGURE 1 | PCA results for specific vital rates to capture individual life histories. Each panel corresponds to a density scenario. Top most panel is for $N = 0$ case, followed by $N = K/2$, and $N = K$. Here *Juv. Survival* and *Ad. Survival* correspond to average survival for individuals before and after they reach their asymptotic size, respectively. Growth is the average proportional growth increment from one time to next for individuals, and reproduction is the average reproductive output.

for mother's body size (scaled by SSD) varies substantially at low and high density. At low population density, mothers of a wide range of body size contribute to reproduction. However, as density increases the range of mothers body size decreased and only mothers of prime body sizes contribute to reproduction (contributing to lower R_0). Thus, as density increases, there is a concentration towards individuals of large prime sizes (average body size 21.82 kg) and contribution from individuals of sizes between 12 and 20 kg is diminished (Figure A9).

While average mother's size increases at high densities, the offspring size at high densities is reduced to an average body size of 12 kg from 15 kg at low density (Figure 4). The reduction in offspring size at high population densities may be understood as an response to the increased competition and resource limitation characteristic of high-density environments.

We also examine the variation in SSD and mother's size distribution at three population sizes ($N = 0$, $N = K/2$ and $N = K$). Since we are interested in sizes (stages), we examine the SSD for size-based matrix population model. For each sample of parameter set, we estimate the equilibrium size K and calculate the stable stage (size) distribution (Figure A8). We take the average of SSD over 250 of our samples. Then we repeat by setting the population size at 0 and at $K/2$. As population size increases from 0 to equilibrium population size K, the proportion of adults increases and the proportion of juveniles decreases, in contrast with density-independent case which has a higher proportion of juveniles (Figure A8).

Lastly, we examine the relationship between R_0 at density-independence (by setting $N = 0$ to evaluate the matrices) and the equilibrium size K for the parameter sets. Figure A10 shows that

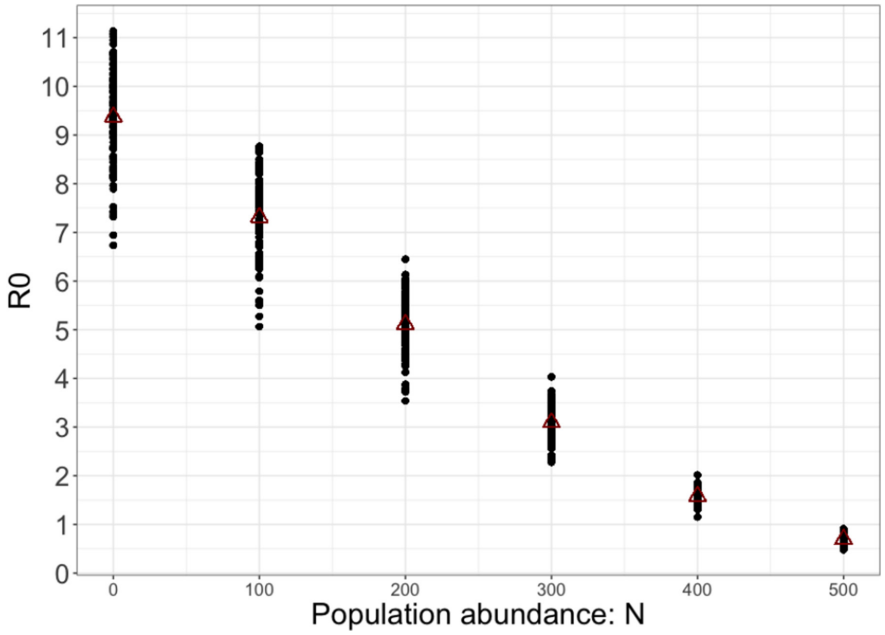

FIGURE 2 | R_0 as a function of population size. Each black point represents the R_0 for a life history evaluated at the particular population size. The red triangle denotes the mean of the 250 life histories from the covariance matrix.

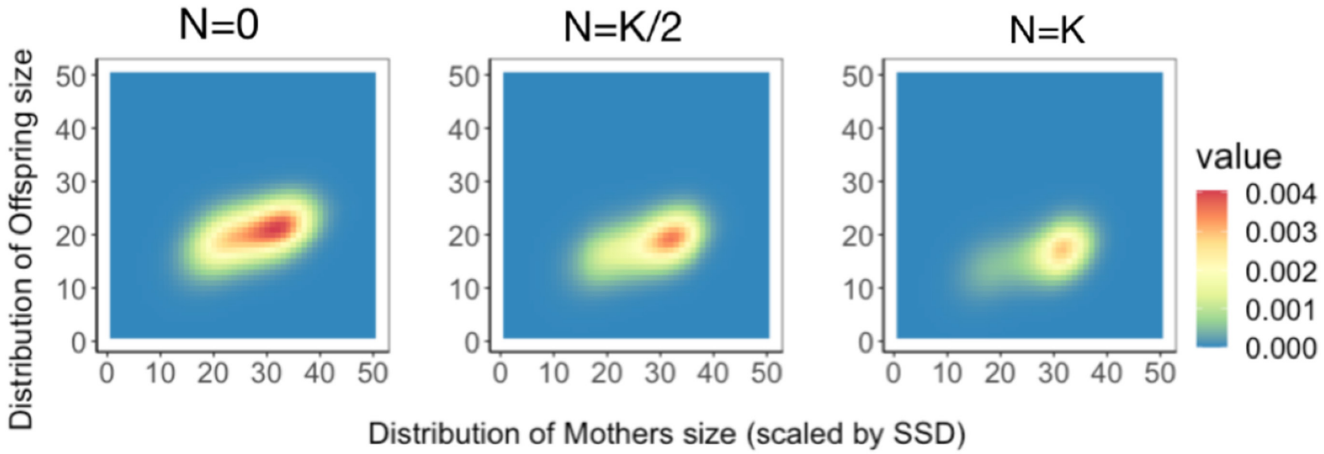

FIGURE 3 | Plot for the distribution of mothers body size at different population densities: The x-axis depicts mother's body size distribution scaled by SSD. The y-axis depicts the offspring body size. Each panel corresponds to a population density scenario (left to right $N = 0, N = K/2, N = K$).

K and R_0 are slightly negatively correlated as found in Kentie et al. (2020). Our results align with (Pande et al. 2020; Pande, Tsubery, and Shnerb 2022) as they show mean population growth rate when rare (a measure of invasibility Chesson 2003) is limited in its use as a metric for persistence.

3.3 | Variation in LRS Trajectories at Different Densities

We calculate the distribution of LRS Tuljapurkar et al. (2020) for the life histories sampled from the covariance matrix. From Lomnicki (1978) work, we hypothesize a higher variation in the distribution of LRS among females at high density compared to low density. However, our results are different from Lomnicki's prediction (Figure 5). The LRS trajectories show considerable variation at $N = 0$ evident from the empirical confidence intervals in Figure 5. However, the variation is constrained at high density, contrary to Lomnicki's prediction. Interestingly, the shape of the LRS distribution varies remarkably at the three density scenarios.

For animals, the probability of having zero offspring corresponds to juvenile mortality. At the $N = K$ panel in Figure 5, the probability of having zero offspring is higher in comparison with case when $N = 0$. These results are consistent with empirical observations since field studies find higher juvenile mortality at equilibrium population sizes than at low densities.

To further examine the LRS distributions, we generated life histories where survival parameters (s_0, s_1, s_2) are sampled from the covariance matrix and the rest of the 13 parameters are fixed to their mean values. Similarly, we fixed all

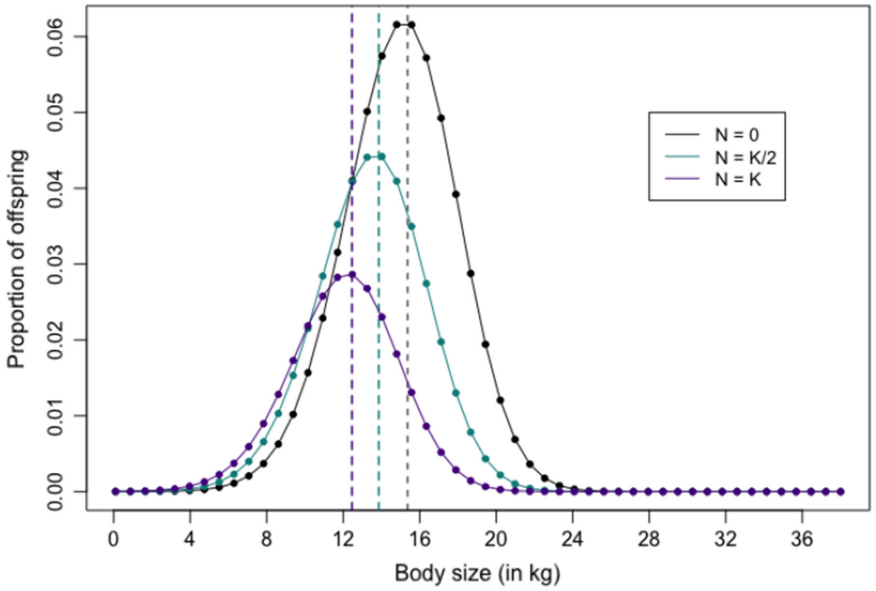

FIGURE 4 | Plot for proportion of offspring' body size. Each colour corresponds to $N = 0$, $N = K/2$ and $N = K$. The vertical lines represent the average body size for that population density.

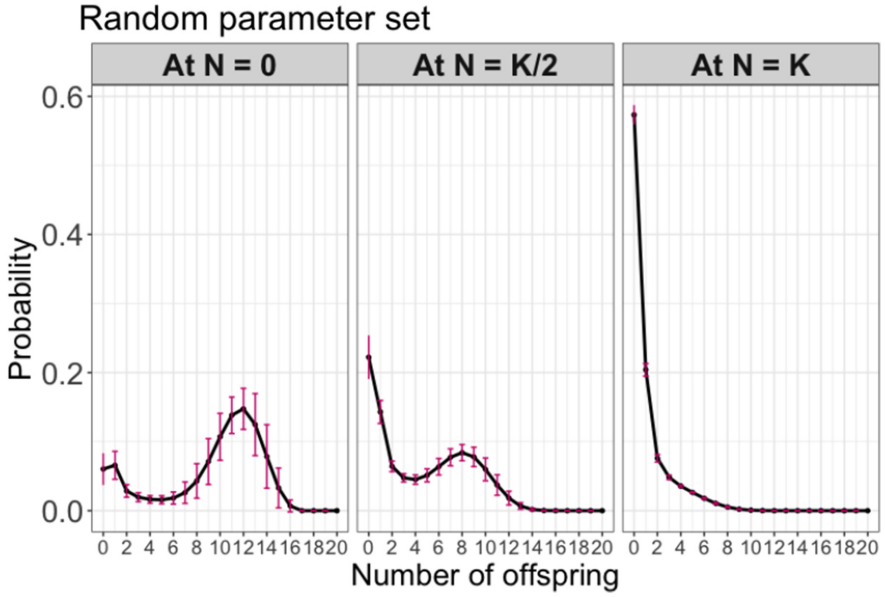

FIGURE 5 | Distribution of LRS for life histories sampled from the covariance matrix at different population densities. The black line depicts the average distribution over life histories, and the pink lines show the empirical confidence intervals.

parameters to their mean values but reproduction parameters (r_0, r_1, r_2). The top panel of Figure A13 shows the average distribution of LRS and the confidence intervals for each offspring number. In the bottom panel of A13, we find at low population density and despite fixed survival, small variation in fertility by chance alone can lead to higher or lower probability of having zero offspring. Finally, we fixed all parameters but growth parameters. Our expectation was the additive effect of survival (only) and growth (only) would be greater than the effect of varying both survival and growth parameters together. We provide slight evidence for such a trade-off for low offspring (0, 1 and 2) but further analysis is needed to uncover the trade-off (Figure A12).

Lastly, we examined the relationship between life-history traits and mean LRS conditional on making at least one offspring (γ). We evaluate average juvenile survival (weighted by SSD) for our parameter set and regress against γ evaluated at the three population sizes (Figure A11). We find that the results are not statistically significant but we find evidence for life histories being constrained at high density compared to low density (Figure A11).

4 | Discussion

We examine the interplay between life-history trade-offs and changes in density in Soay sheep. We use data from Kentie

et al. (2020) to generate life histories and find strong evidence for a negative correlation (trade-off) between survival and growth during the juvenile stage at low density (Figures 1 and A4). The negative correlation and its explanatory power increase with density. The trade-off is not static with respect to population density. At carrying capacity ($N = K$), a new trade-off arises between reproduction and juvenile survival and forms life-history variation within the population. Thus, not all vital rates are equally impacted by changes in density. At low density, the demographic trade-off between growth and survival during the juvenile stage is the main axis of life-history variation among individuals within population and aligns individuals along a slow-fast continuum similarly to what has been consistently reported across species (Stearns 1983; Oli 2004; Gaillard et al. 2016; Jiang et al. 2022; Van de Walle et al. 2023; Salguero-Gómez et al. 2016).

Our findings are consistent with the theory of life-history evolution (Stearns 1992) in that we find the evidence for trade-offs which prevent individuals from being proficient at both surviving and growing to large sizes. However, this markedly differs from previous analyses of intraspecific variation in life histories of vertebrates, which reported a lack of structuring axis of variation among individual life histories and no support for a slow-fast continuum (Van de Walle et al. 2023). This discrepancy might come from the absence of control for density dependence in previous studies. Alternatively, our simulated individual life histories might have included vital rate combinations that might have not been possible to observe in real individuals. Future work comparing potential (as investigated here) and realised (as analysed by Van de Walle et al. 2023) variation in individual life-history strategies should explain this discrepancy.

Our results align with Kentie et al. (2020) as we find that individuals with an average life history cannot simultaneously maximise fitness for both high- and low-density environments. This is because demographic measures such as average survival, reproduction at SSD and distribution of LRS are highly constrained at high population densities (Figure A13). The level of variation and diversity at low population densities is not maintained at high population densities. Ozgul et al. (2009) found population density and maternal body size explain significant amounts of variation in temporal trends of mean body weight in Soay sheep. We find the contribution to reproduction at high population density comes from females of prime adult size. However, at low densities reproductive contribution is from females of both small and large sizes. There is a concentration of individuals of prime size at high densities (Figure A8) for stable stage distribution. An increase in density may be a double whammy for females of small sizes since there is more competition and less individuals contribute to reproduction.

Our finding for probability of reproductive failure supports empirical evidence within Soay sheep population in the wild. At low density, juvenile mortality in Soay sheep is lower than juvenile mortality at high density. Our research finds evidence for density-dependent effects on reproductive effort in natural populations and aligns with r-K selection theory (Bassar et al. 2013). Our research predicts how density-dependent influences strongly shape the distribution of LRS and can lead to density-dependent selection since LRS is an important component of individual fitness. The decreasing complexity in life history variation at the highest density does not support Lomnicki's prediction (Lomnicki 1978). We find perhaps resource limitation constrains the size distribution of females in population, which thereby restrict individual variation in vital rates and demographic outcomes.

There is empirical evidence for links between life-history trade-offs and density-dependent selection from Drosophila cultures (Mueller and Ayala 1981; Mueller, Guo, and Ayala 1991), insects (Gilbert and Manica 2010) and fisheries (Goodwin et al. 2006; Eikeset et al. 2016; Christie et al. 2018, among others). Mueller and Ayala (1981) studied populations of *Drosophila melanogaster* kept at low population densities (r-populations for about 200 generations) and then placed them in crowded cultures (K-populations). They found after 25 generations the K-populations showed higher growth rates and productivity at high densities (relative to the controls), but lower growth rates at low densities and experimentally confirmed fitness trade-offs can arise from density-dependent selection. A study (Sæther et al. 2016) on great tits *Parus major* showed females laying the largest clutch sizes at small population sizes experienced the greatest density-dependent reductions in fitness at large population sizes, thus providing empirical support for r- and K-selection. At small population sizes, phenotypes with large growth rates are favoured, whereas phenotypes with high competitive skills are favoured when populations are close to the carrying capacity K. Travis et al. (2023) provide a comprehensive review of density-dependent selection and how it may promote contrasting patterns of trait means at different population densities.

Author Contributions

H.J. performed analyses and writing. H.J., W.Z., R.K., J.M.G., T.C. and S.T. contributed ideas. W.Z., R.K., J.M.G., T.C. and S.T. contributed analyses and writing. R.K. and T.C. contributed data.

Acknowledgements

H.J. would like to thank Bing-Ehrlich Fellowship and Stanford University for their funding. W.Z. and S.T. would like to thank Stanford University for their funding. J.M.G. would like to thank the ANR project DivInT (ANR-22-CE02-0020) and T.C. would like to thank the University of Oxford, respectively, for their funding.

Data Availability Statement

The data and code that support the findings of this study are publicly available on Zenodo at the link. The zenodo url is https://zenodo.org/records/13755975.

Peer Review

The peer review history for this article is available at https://www.webofscience.com/api/gateway/wos/peer-review/10.1111/ele.14551.

References

Agrawal, A. A., J. K. Conner, and S. Rasmann. 2010. "Tradeoffs and Negative Correlations in Evolutionary Ecology." *Evolution Since Darwin: The First* 150: 243–268.

Bassar, R. D., D. Z. Childs, M. Rees, S. Tuljapurkar, D. N. Reznick, and T. Coulson. 2016. "The Effects of Asymmetric Competition on the Life History of Trinidadian Guppies." *Ecology Letters* 19, no. 3: 268–278.

Bassar, R. D., A. Lopez-Sepulcre, D. N. Reznick, and J. Travis. 2013. "Experimental Evidence for Density-Dependent Regulation and Selection on Trinidadian Guppy Life Histories." *American Naturalist* 181, no. 1: 25–38.

Bell, G., and V. Koufopanou. 1991. "The Architecture of the Life Cycle in Small Organisms." *Philosophical Transactions of the Royal Society of London. Series B: Biological Sciences* 332, no. 1262: 81–89.

Brooks, M. E., K. Kristensen, M. R. Darrigo, et al. 2019. "Statistical Modeling of Patterns in Annual Reproductive Rates." *Ecology* 100, no. 7: e02706.

Cabana, G., and D. L. Kramer. 1991. "Random Offspring Mortality and Variation in Parental Fitness." *Evolution* 45, no. 1: 228–234.

Chesson, P. 2003. "Quantifying and Testing Coexistence Mechanisms Arising From Recruitment Fluctuations." *Theoretical Population Biology* 64, no. 3: 345–357.

Christie, M. R., G. G. McNickle, R. A. French, and M. S. Blouin. 2018. "Life History Variation Is Maintained by Fitness Trade-Offs and Negative Frequency-Dependent Selection." *Proceedings of the National Academy of Sciences* 115, no. 17: 4441–4446.

Clutton-Brock, T. H., I. R. Stevenson, P. Marrow, A. D. MacColl, A. I. Houston, and J. M. McNamara. 1996. "Population Fluctuations, Reproductive Costs and Life-History Tactics in Female Soay Sheep." *Journal of Animal Ecology* 65: 675–689.

Coulson, T., T. G. Benton, P. Lundberg, S. R. X. Dall, B. E. Kendall, and J. M. Gaillard. 2006. "Estimating Individual Contributions to Population Growth: Evolutionary Fitness in Ecological Time." *Proceedings of the Royal Society B: Biological Sciences* 273, no. 1586: 547–555.

Coulson, T. 2012. "Integral Projections Models, Their Construction and Use in Posing Hypotheses in Ecology." *Oikos* 121, no. 9: 1337–1350.

Coulson, T., S. Albon, J. Pilkington, and T. Clutton-Brock. 1999. "Small-Scale Spatial Dynamics in a Fluctuating Ungulate Population." *Journal of Animal Ecology* 68: 658–671.

Coulson, T., E. A. Catchpole, S. D. Albon, et al. 2001. "Age, Sex, Density, Winter Weather, and Population Crashes in Soay Sheep." *Science* 292, no. 5521: 1528–1531.

Czesak, M. E., and C. W. Fox. 2003. "Evolutionary Ecology of Egg Size and Number in a Seed Beetle: Genetic Trade-Off Differs Between Environments." *Evolution* 57, no. 5: 1121–1132.

Descamps, S., J.-M. Gaillard, S. Hamel, and N. G. Yoccoz. 2016. "When Relative Allocation Depends on Total Resource Acquisition: Implication for the Analysis of Trade-Offs." *Journal of Evolutionary Biology* 29, no. 9: 1860–1866.

Dobzhansky, T. 1950. "Evolution in the Tropics." *American Scientist* 38, no. 2: 209–221.

Eikeset, A. M., E. S. Dunlop, M. Heino, G. Storvik, N. C. Stenseth, and U. Dieckmann. 2016. "Roles of Density-Dependent Growth and Life History Evolution in Accounting for Fisheries-Induced Trait Changes." *Proceedings of the National Academy of Sciences* 113, no. 52: 15030–15035.

Ellner, S., D. Childs, and M. Rees. 2016. *Data-Driven Modelling of Structured Populations. A Practical Guide to the Integral Projection Model*. Cham, Switzerland: Springer.

Gaillard, J.-M., J.-F. Lemaître, V. Berger, et al. 2016. "Life Histories, Axes of Variation." In *The Encyclopedia of Evolutionary Biology*, edited by R. Kliman, 312–323. Amsterdam, The Netherlands: Elsevier, Academic Press. https://hal-univ-lyon1.archives-ouvertes.fr/hal-02099457.

Gilbert, J. D. J., and A. Manica. 2010. "Parental Care Trade-Offs and Life-History Relationships in Insects." *American Naturalist* 176, no. 2: 212–226.

Goodwin, N. B., A. Grant, A. L. Perry, N. K. Dulvy, and J. D. Reynolds. 2006. "Life History Correlates of Density-Dependent Recruitment in Marine Fishes." *Canadian Journal of Fisheries and Aquatic Sciences* 63, no. 3: 494–509.

Grenfell, B. T., OF Price, S. D. Albon, and T. H. Glutton-Brock. 1992. "Overcompensation and Population Cycles in an Ungulate." *Nature* 355, no. 6363: 823–826.

Hodgson, D. J., and S. Townley. 2004. "Methodological Insight: Linking Management Changes to Population Dynamic Responses: The Transfer Function of a Projection Matrix Perturbation." *Journal of Applied Ecology* 41, no. 6: 1155–1161.

Horvitz, C., D. W. Schemske, and H. Caswell. 1997. "The Relative "Importance" of Life-History Stages to Population Growth: Prospective and Retrospective Analyses." In *Structured-Population Models in Marine, Terrestrial, and Freshwater Systems*, edited by S. Tuljapurkar and H. Caswell, 247–271. Boston, MA: Springer.

Jiang, S., H. Jaggi, W. Zuo, et al. 2022. "Reproductive Dispersion and Damping Time Scale With Life-History Speed." *Ecology Letters* 25, no. 9: 1999–2008.

Kentie, R., S. M. Clegg, S. Tuljapurkar, J.-M. Gaillard, and T. Coulson. 2020. "Life-History Strategy Varies With the Strength of Competition in a Food-Limited Ungulate Population." *Ecology Letters* 23, no. 5: 811–820.

King, J. R., and D. A. Jackson. 1999. "Variable Selection in Large Environmental Data Sets Using Principal Components Analysis." *Environmetrics: The Official Journal of the International Environmetrics Society* 10, no. 1: 67–77.

Lomnicki, A. 1978. "Individual Differences Between Animals and the Natural Regulation of Their Numbers." *Journal of Animal Ecology* 47: 461–475.

MacArthur, R. H. 1962. "Some Generalized Theorems of Natural Selection." *Proceedings of the National Academy of Sciences* 48, no. 11: 1893–1897.

Metcalf, C., and E. Jessica. 2016. "Invisible Trade-Offs: Van Noordwijk and de Jong and Life-History Evolution." *American Naturalist* 187, no. 4: iii.

Mueller, L. D., and F. J. Ayala. 1981. "Trade-Off Between r-Selection and K-Selection in Drosophila Populations." *Proceedings of the National Academy of Sciences* 78, no. 2: 1303–1305.

Mueller, L. D., P. Guo, and F. J. Ayala. 1991. "Density-Dependent Natural Selection and Trade-Offs in Life History Traits." *Science* 253, no. 5018: 433–435.

Norris, K., and M. R. Evans. 2000. "Ecological Immunology: Life History Trade-Offs and Immune Defense in Birds." *Behavioral Ecology* 11, no. 1: 19–26.

Oli, M. K. 2004. "The Fast-Slow Continuum and Mammalian Life-History Patterns: An Empirical Evaluation." *Basic and Applied Ecology* 5, no. 5: 449–463.

Ozgul, A., S. Tuljapurkar, T. G. Benton, J. M. Pemberton, T. H. Clutton-Brock, and T. Coulson. 2009. "The Dynamics of Phenotypic Change and the Shrinking Sheep of St. Kilda." *Science* 325, no. 5939: 464–467.

Pande, J., T. Fung, R. Chisholm, and N. M. Shnerb. 2020. "Mean Growth Rate When Rare Is Not a Reliable Metric for Persistence of Species." *Ecology Letters* 23, no. 2: 274–282.

Pande, J., Y. Tsubery, and N. M. Shnerb. 2022. "Quantifying Invasibility." *Ecology Letters* 25, no. 8: 1783–1794.

Pianka, E. R. 1970. "On r-and K-Selection." *American Naturalist* 104, no. 940: 592–597.

Quintana-Ascencio, P. F., and M. Morales-Hernández. 1997. "Fire-Mediated Effects of Shrubs, Lichens and Herbs on the Demography of Hypericum Cumulicola in Patchy Florida Scrub." *Oecologia* 112: 263–271.

Reznick, D., M. Bryant, and D. Holmes. 2006. "The Evolution of Senescence and Post-Reproductive Lifespan in Guppies (Poecilia Reticulata)." *PLoS Biology* 4, no. 1: 136.

Roff, D. A. 1992. *The Evolution of Life Histories: Theory and Analysis*. London, UK: Springer.

Roughgarden, J. 1971. "Density-Dependent Natural Selection." *Ecology* 52, no. 3: 453–468.

Sæther, B.-E., M. E. Visser, V. Grøtan, and S. Engen. 2016. "Evidence for r-and K-Selection in a Wild Bird Population: A Reciprocal Link Between Ecology and Evolution." *Proceedings of the Royal Society B: Biological Sciences* 283, no. 1829: 20152411.

Salguero-Gómez, R., O. R. Jones, E. Jongejans, et al. 2016. "Fast-Slow Continuum and Reproductive Strategies Structure Plant Life-History Variation Worldwide." *Proceedings of the National Academy of Sciences* 113, no. 1: 230–235.

Simmonds, E. G., and T. Coulson. 2015. "Analysis of Phenotypic Change in Relation to Climatic Drivers in a Population of Soay Sheep Ovis Aries." *Oikos* 124, no. 5: 543–552.

Smith, C. C., and S. D. Fretwell. 1974. "The Optimal Balance Between Size and Number of Offspring." *American Naturalist* 108, no. 962: 499–506.

Stearns, S. C. 1983. "The Influence of Size and Phylogeny on Patterns of Covariation Among Life-History Traits in the Mammals." *Oikos* 41: 173–187.

Stearns, S. C. 1989. "Trade-Offs in Life-History Evolution." *Functional Ecology* 3, no. 3: 259–268.

Stearns, S. C. 1992. *The Evolution of Life Histories*. Oxford: Oxford University Press.

Steiner, U. K., S. Tuljapurkar, and T. Coulson. 2014. "Generation Time, Net Reproductive Rate, and Growth in Stage-Age-Structured Populations." *American Naturalist* 183, no. 6: 771–783.

Tatarenkov, A., C. I. M. Healey, G. F. Grether, and J. C. Avise. 2008. "Pronounced Reproductive Skew in a Natural Population of Green Swordtails, *Xiphophorus helleri*." *Molecular Ecology* 17, no. 20: 4522–4534.

Travis, J., R. D. Bassar, T. Coulson, D. Reznick, and M. Walsh. 2023. "Density-Dependent Selection." *Annual Review of Ecology, Evolution, and Systematics* 54: 85–105.

Tuljapurkar, S., W. Zuo, T. Coulson, C. Horvitz, and J.-M. Gaillard. 2020. "Skewed Distributions of Lifetime Reproductive Success: Beyond Mean and Variance." *Ecology Letters* 23, no. 4: 748–756.

Tuljapurkar, S., W. Zuo, T. Coulson, C. Horvitz, and J.-M. Gaillard. 2021. "Distributions of LRS in Varying Environments." *Ecology Letters* 24, no. 7: 1328–1340.

Van de Walle, J., R. Fay, J. M. Gaillard, et al. 2023. "Individual Life Histories: Neither Slow nor Fast, Just Diverse." *Proceedings of the Royal Society B* 290, no. 2002: 20230511.

Van Noordwijk, A. J., and G. De Jong. 1986. "Acquisition and Allocation of Resources: Their Influence on Variation in Life History Tactics." *American Naturalist* 128, no. 1: 137–142.

Venable, D. L. 1992. "Size-Number Trade-Offs and the Variation of Seed Size With Plant Resource Status." *American Naturalist* 140, no. 2: 287–304.

Zera, A. J., and L. G. Harshman. 2001. "The Physiology of Life History Trade-Offs in Animals." *Annual Review of Ecology and Systematics* 32, no. 1: 95–126.

Appendix A

TABLE A1 | The table provides a list of 16 parameters we use for the four IPM functions (Coulson 2012).

Parameter	Description
s_0	Survival: intercept
s_1	Survival: slope body mass
s_2	Survival: slope population size
r_0	Reproduction intercept
r_1	Reproduction: slope body mass
r_2	Reproduction: slope population density
γ_0	Development, mean: intercept
γ_1	Development, mean: slope body mass
γ_2	Development, mean: slope population size
γ_3	Development, variance: intercept
γ_4	Development, variance: slope body mass
δ_0	Inheritance, mean: intercept
δ_1	Inheritance, mean; slope body mass
δ_2	Inheritance, mean: slope population size
δ_3	Inheritance, variance: intercept
δ_4	Inheritance, variance: slope body mass

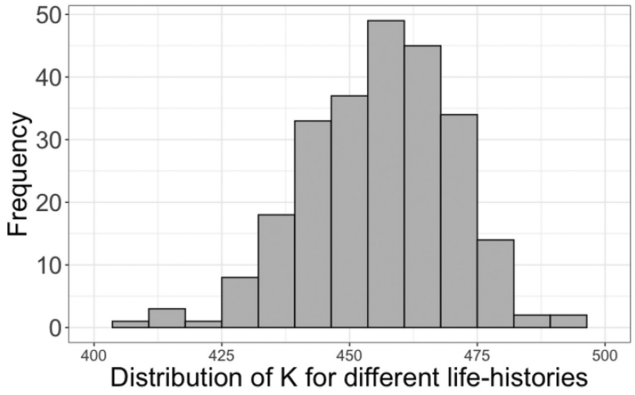

FIGURE A1 | Histogram of equilibrium population size or carrying capacity (K). The mean carrying capacity across all life histories is 454.

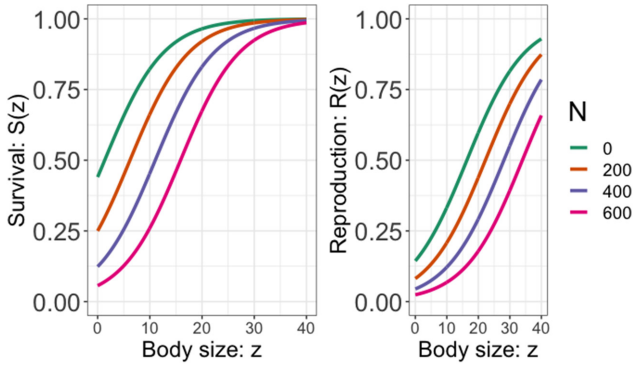

FIGURE A2 | Plot of survival and reproduction functions for different values of population size, N.

	PC1	PC2	PC3	PC4	N
Juv. Survival	-0.6879697	0.12862049	0.1212322	-0.7038872	0
Ad. Survival	-0.686233	-0.0630279	0.2061516	0.69470369	0
Reproduction	-0.2023425	-0.6648947	-0.7174507	-0.047297	0
Growth	0.1218173	-0.7330752	0.65426962	-0.1403301	0
Juv. Survival	0.68750662	-0.0194718	0.39635595	-0.6081591	K/2
Ad. Survival	0.68088722	0.20812351	-0.1056572	0.69420008	K/2
Reproduction	0.04627893	0.72806789	-0.585899	-0.3528424	K/2
Growth	-0.2481642	0.65285726	0.69889976	0.15404882	K/2
Juv. Survival	-0.6428758	0.01294431	-0.1599549	0.74897098	K
Ad. Survival	0.25436365	-0.7802743	-0.560259	0.11216476	K
Reproduction	0.61068116	-0.0551793	0.4797481	0.62758707	K
Growth	0.38610661	0.62286408	-0.6560229	0.18054366	K

FIGURE A3 | Table of PCA loadings for the principal components.

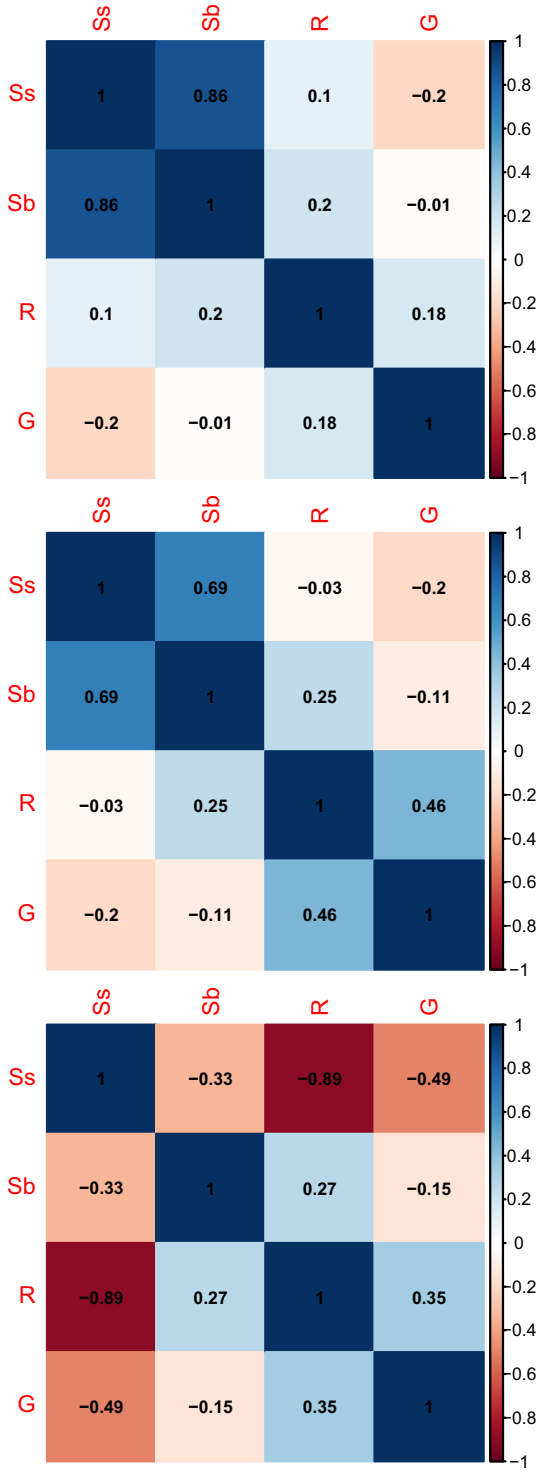

FIGURE A4 | Correlation matrices for the three population densities. The top most panel corresponds to $N = 0$, the middle panel corresponds to $N = K/2$, and the bottom panel corresponds to $N = K$. The colours red, blue and white correspond to negative, positive and no correlation.

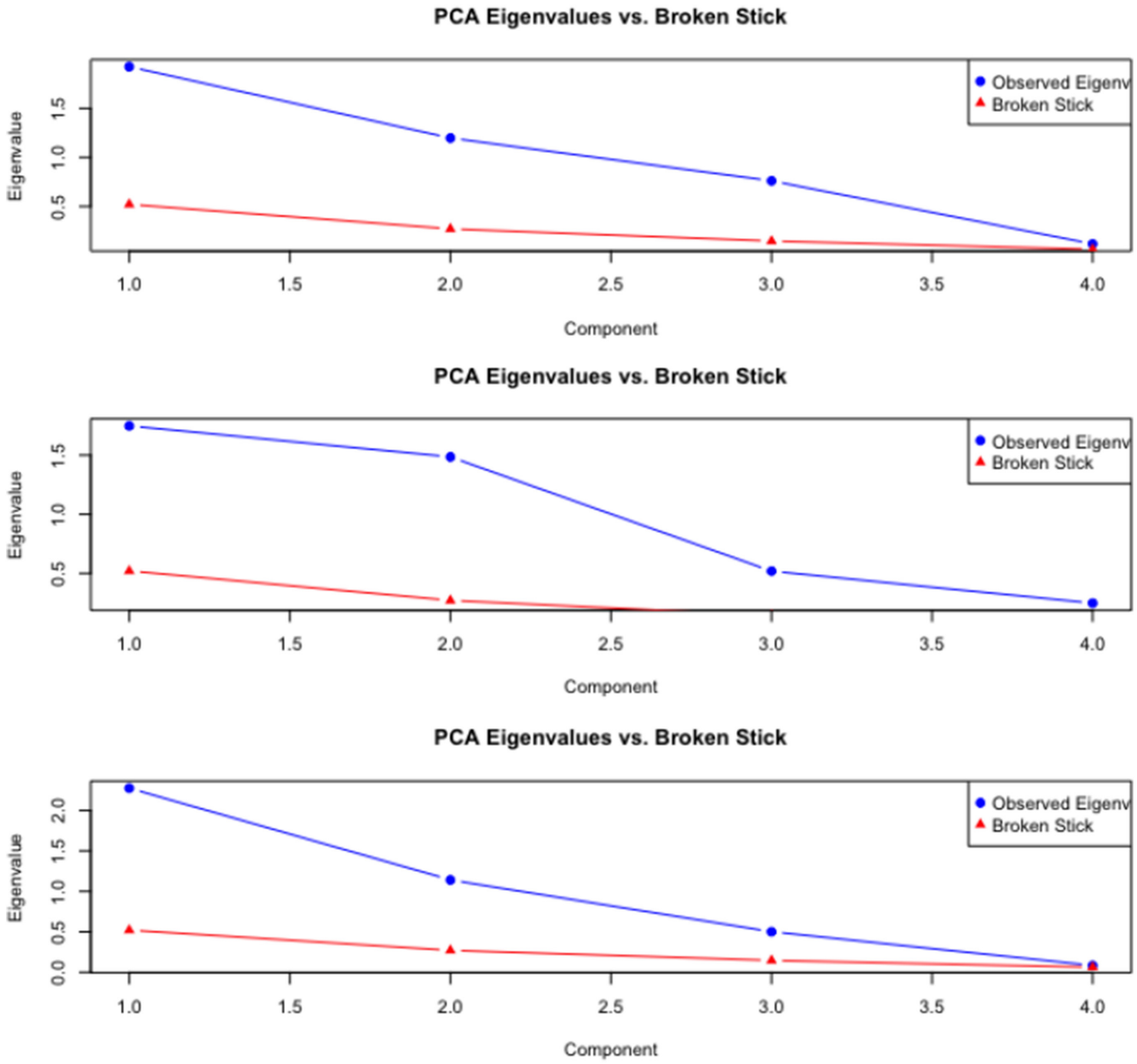

FIGURE A5 | Eigenvalues from data and broken stick model. The top most panel corresponds to $N = 0$, followed by $N = K / 2$, and $N = K$. Blue corresponds to observed eigenvalues from the data and red corresponds to eigenvalues from the broken stick model.

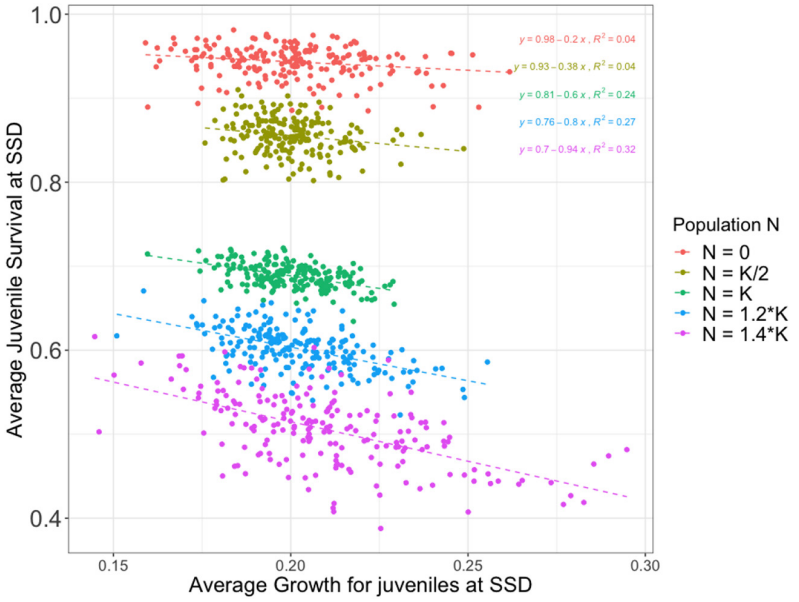

FIGURE A6 | Plot for negative association between average growth increment for juveniles at SSD on the x-axis and average juvenile survival at SSD on the y-axis. The colours correspond to population density at $N = 0$, $N = K/2$, $N = K$, $N = (1.2)K$ and $N = (1.4)K$.

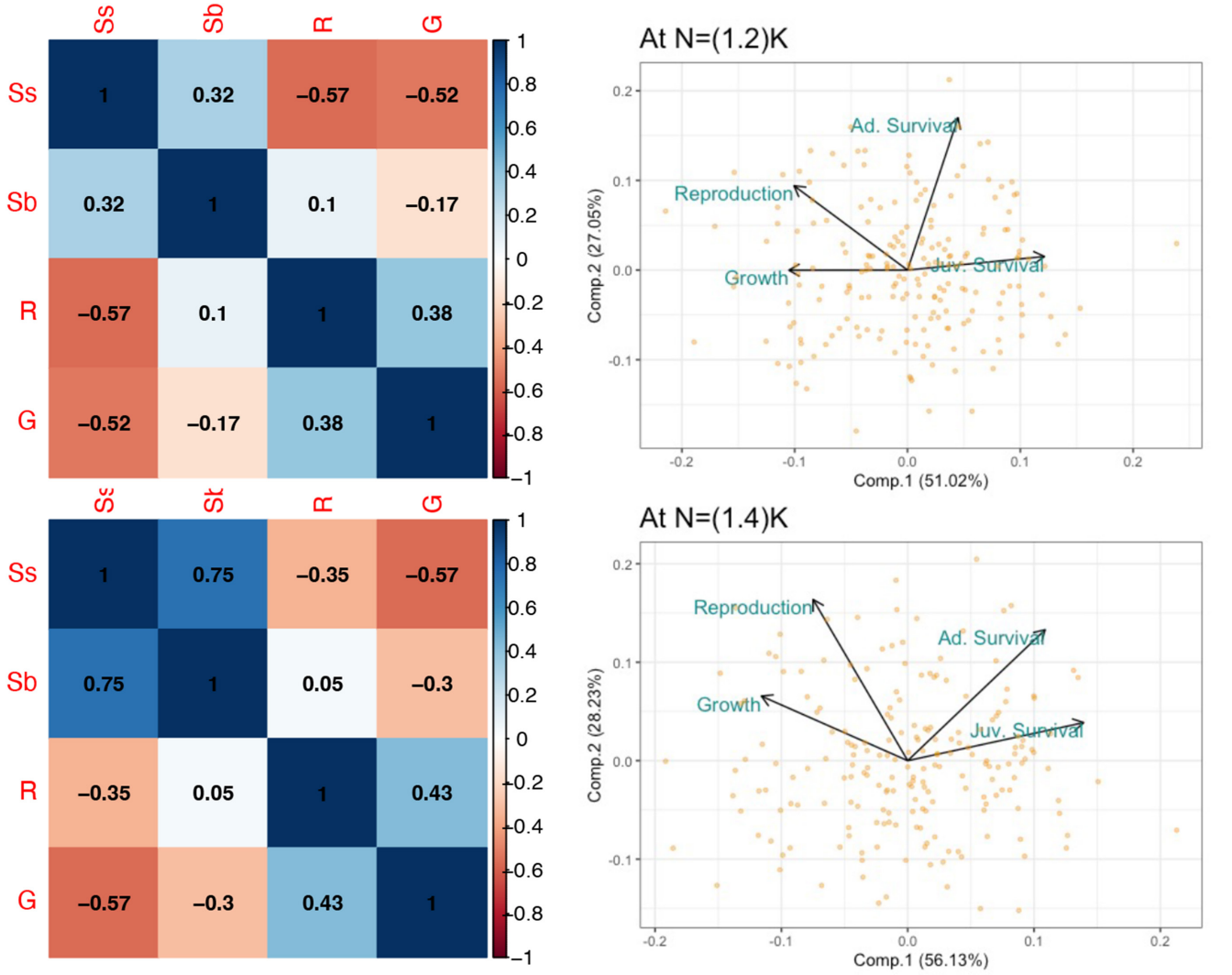

FIGURE A7 | The top two panels show the correlation matrix and corresponding PCA at $N = 1.2K$. The bottom panels correspond to $N = 1.4K$. The colours red, blue and white correspond to negative, positive and no correlation.

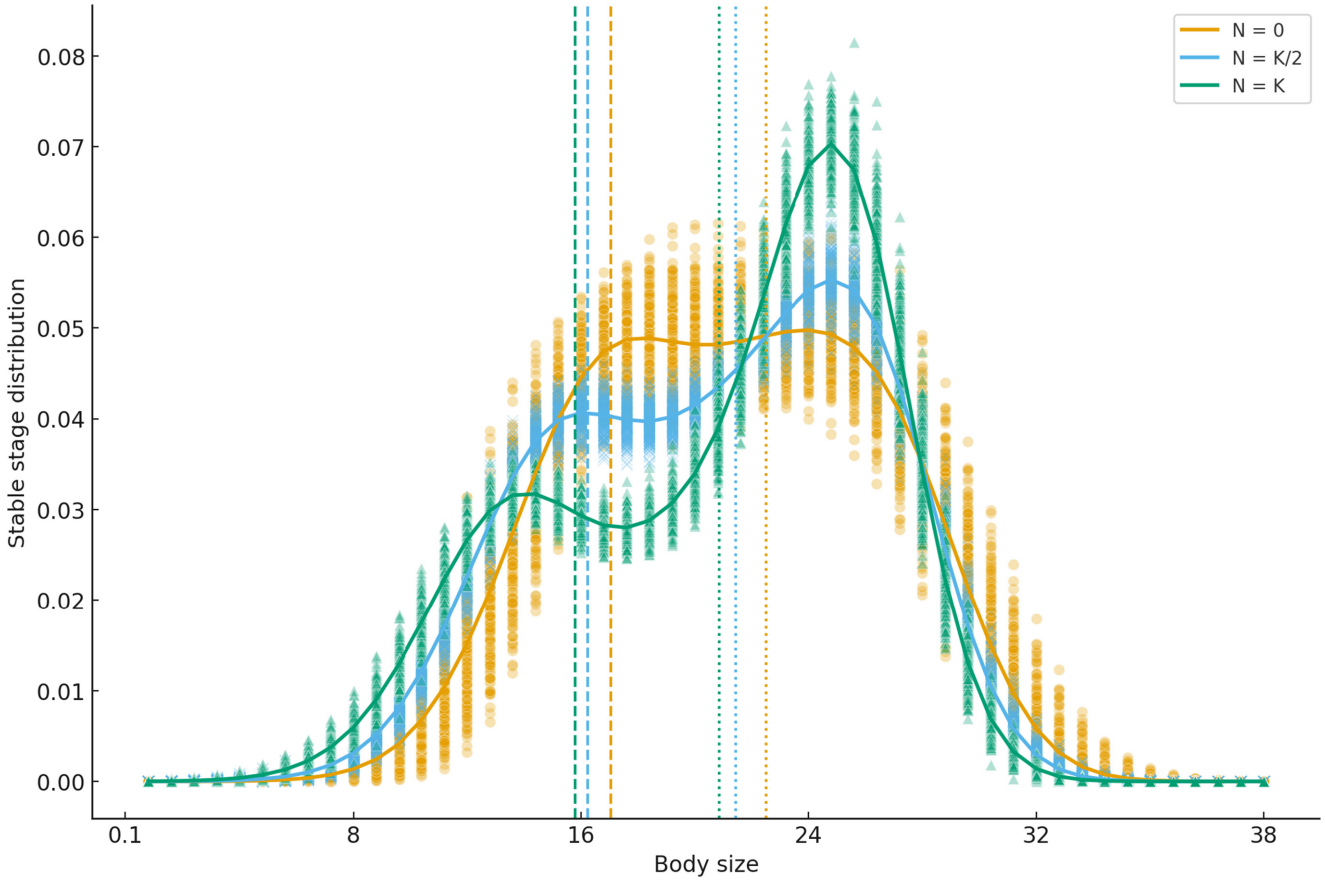

FIGURE A8 | Stable stage distribution at different population size. The legend corresponds to $N = 0$, $N = K/2$ and $N = K$. The solid line plots the normalised stage distribution on the y-axis and body size on the x-axis. The vertical dotted lines and dashed lines correspond to the average adult body size and the average juvenile body size at different densities. The points in the background correspond to simulations. For $N = K$, ~62% of the population is above the average represented by the vertical line compared to 58% for $N = 0$.

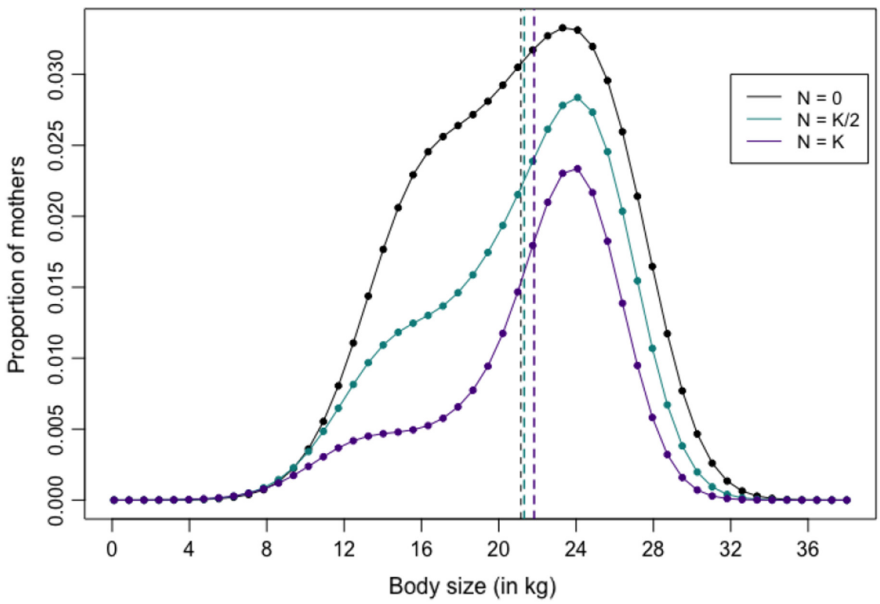

FIGURE A9 | Plot for proportion of mothers' body size. Each colour corresponds to $N = 0$, $N = K/2$ and $N = K$. The vertical lines represent the average body size for that population density.

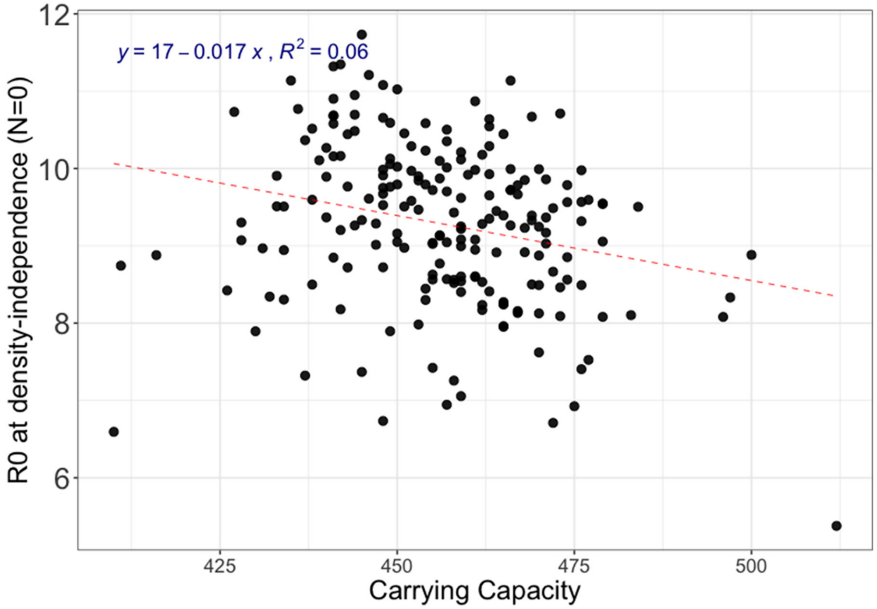

FIGURE A10 | The plot shows negative correlation between carrying capacity, K on the x-axis and R_0 at $N = 0$ on the y-axis.

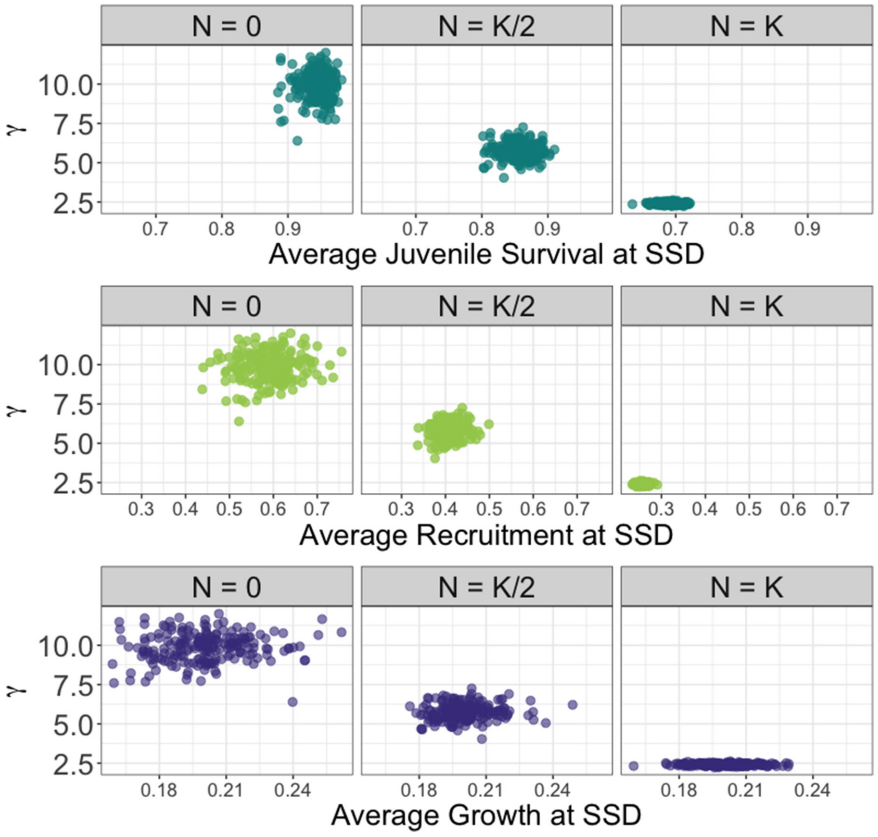

FIGURE A11 | Trends for average vital rates at different population densities. On the y-axis is γ, that is the mean LRS conditional on making at least one offspring. The top three panels (left to right at $N = 0$, $N = K/2$ and $N = K$) have average juvenile survival rates at SSD on the x-axis, the middle panel has average reproduction at SSD, and the bottom three panels have average growth at SSD.

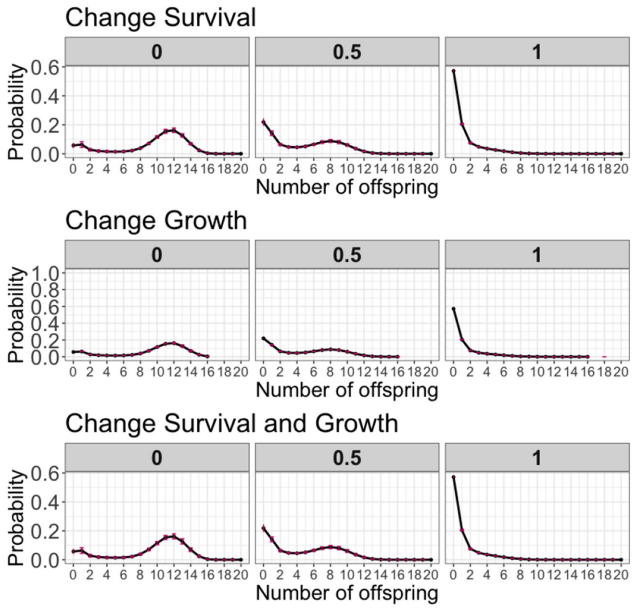

FIGURE A12 | Distribution of LRS when survival and growth parameters are sampled from the covariance matrix at different population densities. The first and second panel correspond to varying survival and growth parameters. The third panel corresponds to varying both survival and growth parameters simultaneously.

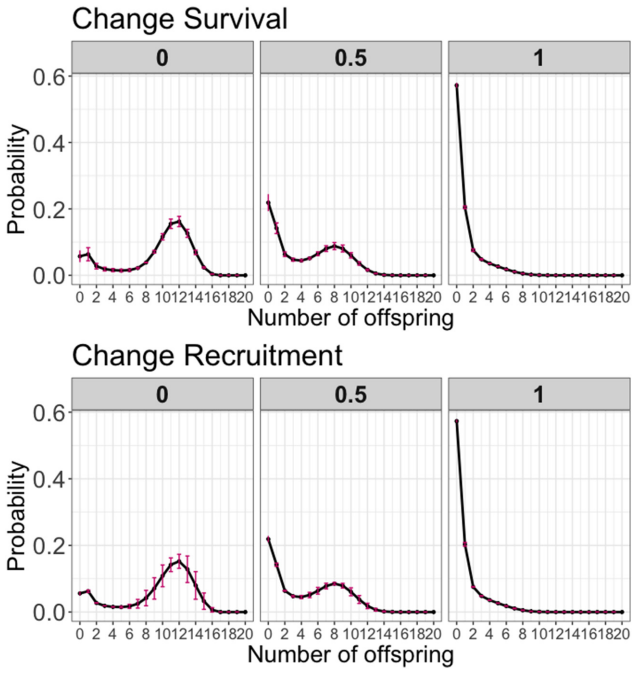

FIGURE A13 | Plot for distribution of LRS. The top-three panels correspond to LRS distribution when only survival parameters are sampled from the covariance matrix and the rest of the parameters are fixed to their mean values. The bottom-three panels correspond to LRS distribution when only reproduction parameters are sampled and the rest of the parameters are fixed to their mean values. Each panel corresponds to a density scenario. Left most panel is for $N = 0$ case, followed by $N = K/2$, and $N = K$.